Water-Current and IMU Aided AUV Localization in Deep Mid-Water

Lashika Medagoda[1] and James C. Kinsey[2]

I. Introduction

Survey class Autonomous Underwater Vehicles (AUVs) typically rely on Doppler Velocity Logs (DVL) for precise navigation near the seafloor. In cases where the distance to the seafloor is greater than the DVL bottom lock range, localizing between the surface where GPS is available and the seafloor presents a localization problem, since both GPS and DVL are unavailable in the mid-water column.

Previous work [3] [6] proposed a solution to navigation in the mid-water column that exploits the stability of the vertical water current profile in space over the minutes scale. With repeated measurements of these currents with the Acoustic Doppler Current Profiler (ADCP) mode of the DVL during vertical descent, along with sensor fusion of other low cost sensors, position error growth is constrained during the dive. Following DVL bottom lock, due to correlations in the joint vehicle and water current velocity estimation, the entire velocity history is further constrained.

Previous work in this area includes [4] to generalize the ADCP-aided filter to horizontal motion, including using ADCP beam geometry and a water-volume grid approach for the water velocity state space. Furthermore, a number of extensions are developed in [5] to improve navigation performance during missions characterized by prolonged time-scales.

In this paper, the ADCP-aided filter is applied to a 25 hour 5000m deep straight line mission, with the environmental effects considered. Also, the addition of IMU acceleration outputs from a navigation grade IMU for the prediction model as an alternative to the constant velocity (CV) model are implemented and analyzed. The re-acquisition of DVL bottom-lock at the end of the mission, simulating the vehicle lowering altitude to within range of the seafloor, is also investigated.

II. Extended Kalman filter with current estimation

Position, velocity, and attitude states are estimated using an EKF. Additionally, ADCP measurement biases for each measurement cell in each beam are estimated, along with the North, East, Down components of the water current velocity. Water velocity states are modeled as nodes in a trilinear interpolated grid, each with an associated velocity vector. The prediction step in this implementation includes a CV model and an IMU-acceleration based model.

Once the state matrix exceeds a certain size due to initializing newly observed water current velocity states, the oldest of these states are marginalized out of the EKF, which involves removing them from the state vector and covariance matrix. This allows constant-time updates as the state vector is not allowed to expand indefinitely and is controlled to a maximum size. In this paper, we use a maximum state vector size of 600, due to the geometry of the beams, resolution of water current gridding, and processing constraints. This is justified as older water current states may no longer be observed, and if they are re-observed, they can be re-initialized instead. Note, it is undesirable to set this maximum size too low as it would result in continuously re-initialized water current velocity states, throwing away correlation information in the filter which could be useful. Further detail regarding the formulation of the filter, sensor models and correlation models can be found in [5].

A. Fusion with IMU Data

The IMU sensor data used in this paper (iXSEA PHINS II) has post-processing applied, as the raw measurements without added noise are not available due to export control. The unit supplies north-referenced attitude utilizing the gravity vector and gyrocompassing. The unit also supplies gravity-compensated acceleration outputs, in our case at 10 Hz. In order to use the acceleration output for our prediction model, the following model is applied:

$$\mathbf{a}_{PHINS} = \mathbf{a}_{true} + \mathbf{b}_a + \nu_a \tag{1}$$

where $\mathbf{a}_{true}$ is the true acceleration of the vehicle, $\mathbf{b}_a$ is the accelerometer bias, and ν_a is zero-mean Gaussian noise. The bias in the accelerometer is modelled as a first-order Markov process:

$$\dot{\mathbf{b}}_a = -\frac{1}{\tau_{b,a}}\mathbf{b}_a + \nu_{b,a} \tag{2}$$

where $\tau_{b,a}$ is a time constant which affects the rate at which the bias changes, and $\nu_{b,a}$ is a random variable with standard deviation [1]

$$\sigma_{bias} = \sqrt{\frac{2f\sigma^2_{bias\,drift}}{\tau_{b,a}}} \tag{3}$$

where $\sigma_{bias\,drift}$ is the standard deviation of the bias in the long term, which can be set as the bias stability specification of the IMU to limit the magnitude of the bias with time, and f is the frequency at which the process model operates. The magnitude of $\tau_{b,a}$ was empirically tuned to a value of 10000 seconds.

[1]Lashika Medagoda (Lashika.Medagoda@dfki.de) is with the German Center for Artificial Intelligence (DFKI). [2]James Kinsey (jkinsey@whoi.edu) is with the Woods Hole Oceanographic Institution.

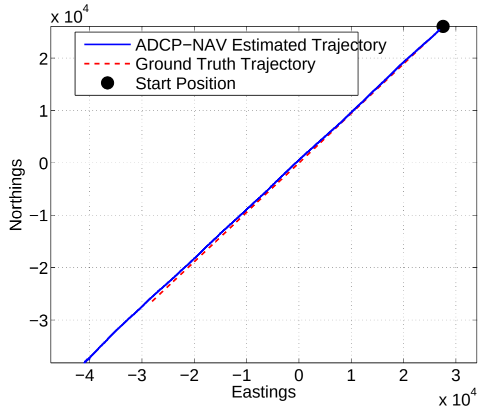

Fig. 1. The estimation result is compared to the ground truth from USBL for Sentry 299.

III. Field Results using the *Sentry* AUV

Our ADCP-aided localization algorithm was validated using data obtained with the *Sentry* AUV on two separate missions. *Sentry* is a 6000m rated AUV designed and built by the Woods Hole Oceanographic Institution (WHOI) for geophysical, geochemical, and biological surveys [2]. The ADCP sensor is a 300 kHz Navigator (RD Instruments, San Diego, CA) with 120m maximum range for water profiling. The process model used for the vehicle is a CV model. The process noise is tuned according to the worst case dynamics possible by the vehicle and no thruster model is incorporated in this experiment. Attitude information is supplied by a PHINS inertial navigation system (IXSEA SAS, Marly-le-Roi, France) used as a gyrocompass, depth is provided by a nano-resolution pressure depth sensor (Paroscientific Inc., Redmond, WA), and USBL measurements are supplied by a Ranger USBL system (Sonardyne International Ltd., Aberdeen, UK). The error metrics used to reject ADCP measurements are an error velocity threshold, percent good reported from sensor, and χ^2 test for normalized innovations.

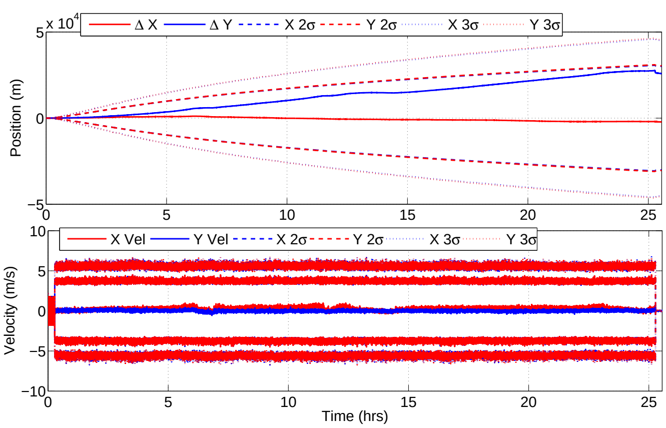

Fig. 2. Results for *Sentry* dives 298 with a constant velocity based prediction model. The top plot shows the position residuals and 2 and 3 σ uncertainty bounds while the lower plot shows the velocity estimate residuals and uncertainty bounds. In the position estimate residuals compared to the ground truth DVL+USBL solution stay within the 2σ uncertainty bounds showing that the filter remains consistent.

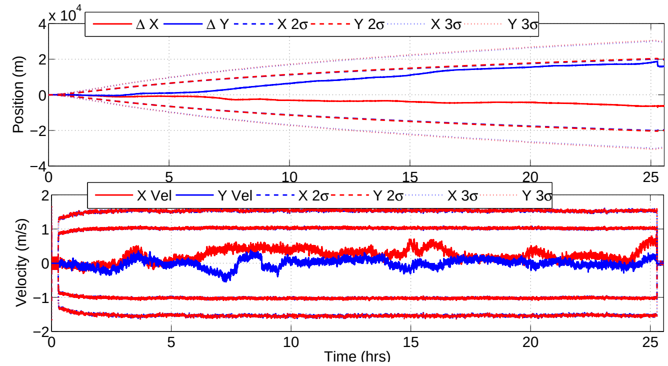

Fig. 3. Results for *Sentry* dives 298 with an IMU based prediction model. As in Figure 2, the top plot shows the position residuals and 2 and 3 σ uncertainty bounds while the lower plot shows the velocity estimate residuals and uncertainty bounds. Again, in the position estimate residuals compared to the ground truth DVL+USBL solution stay within the 2σ uncertainty bounds showing that the filter remains consistent.

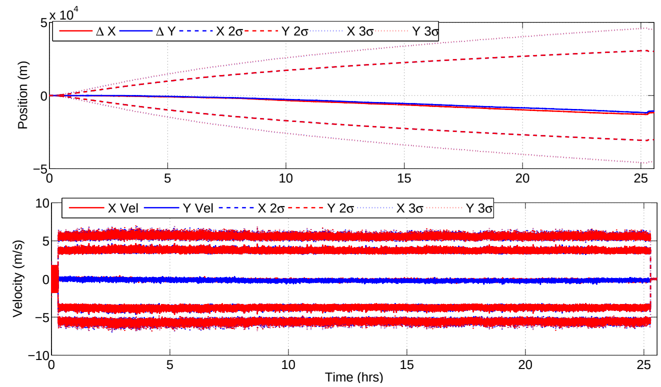

Fig. 4. Results for *Sentry* dives 299 with a constant velocity based prediction model. As in Figure 2, the top plot shows the position residuals and 2 and 3 σ uncertainty bounds while the lower plot shows the velocity estimate residuals and uncertainty bounds. Again, in the position estimate residuals compared to the ground truth DVL+USBL solution stay within the 2σ uncertainty bounds showing that the filter remains consistent.

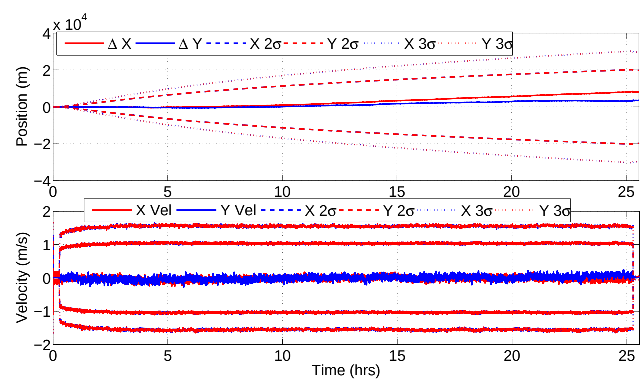

Fig. 5. Results for *Sentry* dives 299 with an IMU based prediction model. As in Figure 2, the top plot shows the position residuals and 2 and 3 σ uncertainty bounds while the lower plot shows the velocity estimate residuals and uncertainty bounds. Again, in the position estimate residuals compared to the ground truth DVL+USBL solution stay within the 2σ uncertainty bounds showing that the filter remains consistent.

Results from two *Sentry* dives are reported here – Sentry298 and Sentry299. These missions are long distance magnetic survey obtaining magnetic measurements in the

Western Pacific Ocean in December 2014 at operating depths of approximately 5000m. Figure 1, shows the mission trajectory — an approximately 80km straight line at 200m above the seafloor, over a period of 25 hours. The experiment uses the DVL and USBL for initialization at the start of the mission, and then data-denies both for 25 hours. After 25 hours, DVL measurements are again processed by the filter to simulate DVL bottom-lock re-acquisition at low altitude. The following compares the results obtained between using the CV prediction model and using IMU acceleration measurements in the process model on the Sentry 298-299 missions.

The results were process on an Intel i7-4771 CPU @ 3.50GHz. The grid size used was 500m in the horizontal direction and 40m in the vertical direction. The processing times for each mission was approximately 7 hours, implying potential real-time application.

One challenging feature of this dataset is the magnitude of the noise in the ADCP measurements, as observed by analysing the error velocity output, which range from 1-3 m/s (2σ). The deep water contains very few scatterers, thus making the return signal particularly weak, as shown through looking at the correlation signal and return signal strength diagnostics. Nevertheless, once the sensor modeling accounts for this uncertainty, in variance and bias uncertainty, the filter behaves in a consistent manner when compared to the USBL ground truth.

Figure 1 shows the estimated mission trajectory versus the ground truth from USBL. Figures 2 shows the position and velocity estimate error and uncertainty for Sentry298 with a CV model, where Figure 3 shows the same with an IMU acceleration based prediction model. The error is within the uncertainty bounds for position and velocity, implying a consistent filter. The total position error grows to 27.5 km (uncertainty 30.9 km 2σ) in the CV model case, compared to 19.7 km (uncertainty 20.4 km 2σ) in the IMU prediction model case. Once DVL bottom-lock is reacquired at the end of the mission, a correction of approximately 1.5km and 2.7km in position occurs for the CV and IMU case respectively. Uncertainty in position after DVL bottom-lock reduces by 0.3km (2σ) for both cases. The velocity uncertainty with a CV model fluctuates above 3.4 m/s (2σ) compared to 1.0 m/s (2σ) with the IMU model.

Figures 4 shows the position estimate error and uncertainty for Sentry299 with a CV model, where Figure 5 shows the same with an IMU acceleration based prediction model. In this case, the total position errors are 17.3 km (uncertainty 30.7 km 2σ) for the CV model case, and 8.8 km (uncertainty 20.2 km 2σ) for the IMU prediction model case. The uncertainties are the same as Sentry298 in position and velocity, as the same models and conditions were applied. Uncertainty in position after DVL bottom-lock also reduces by 0.3km (2σ) in each case. Compared to Sentry298, the error reduction is smaller as the DVL measurement innovations are smaller compared to the prior estimate from the filter (as seen in Figures 4 and 5). In this case, the CV model corrects 1.5 km, while the IMU model has a negligible correction of 37m.

Thus, it appears the addition of the IMU based acceleration prediction model provides approximately one-third reduction in the uncertainty in position, along with a two-thirds reduction in velocity uncertainty.

IV. Future work

The additional incorporation of a dynamic model of the vehicle can improve the accuracy of the method, further reducing the error growth in position during GPS and DVL bottom lock blackout periods. Further extensions based on terrain maps obtained *a priori* or measurements of magnetic field deviations for the purposes of navigation are considered as future work.

References

[1] W.S. Flenniken IV. Modeling inertial measurement units and analyzing the effect of their errors in navigation applications. *Auburn University Masters Thesis*, 2005.

[2] J.C. Kinsey, Q. Yang, and J.C. Howland. Nonlinear dynamic model-based state estimators for underwater navigation of remotely operated vehicles. *IEEE Transactions on Control Systems Technology*, (99):1–1, 2014.

[3] L. Medagoda, M.V. Jakuba, O. Pizarro, and S.B. Williams. Water Column Current Profile Aided Localisation for Autonomous Underwater Vehicles. In *IEEE OCEANS 2010*, May 2010.

[4] L. Medagoda, M.V. Jakuba, O. Pizarro, and S.B. Williams. Water column current aided localisation for significant horizontal trajectories with Autonomous Underwater Vehicles. In *IEEE OCEANS 2011*, pages 1–10. IEEE, May 2011.

[5] L. Medagoda, J.C. Kinsey, and M. Eilders. Autonomous underwater vehicle localization in a spatiotemporally varying water current field. In *Proceedings of the IEEE International Conference on Robotics and Automation*, 2015.

[6] L. Medagoda, Williams S.B., Pizarro O., and Jakuba M.V. Water Column Current Profile Aided Localisation combined with View-based SLAM for Autonomous Underwater Vehicles. In *International Conference on Robotics and Automation 2011*, Shanghai, China, 2011. IEEE.